Atom number calibration in absorption imaging at very small atom numbers

Gregory Konstantinidis, Melina Pappa, Gustav Wikström, Paul Condylis, Daniel Sahagun, Mark D. Baker, Olivier Morizot, Wolf Von Klitzing

Cent. Eur. J. Phys. • 10(5) • 2012 • 1054-1058
DOI: 10.2478/s11534-012-0108-x

VERSITA

Central European Journal of **Physics**

Atom number calibration in absorption imaging at very small atom numbers

Research Article

Gregory O. Konstantinidis[1,2], Melina Pappa[1,2], Gustav Wikström[1], Paul C. Condylis[1,3], Daniel Sahagun[1,3], Mark Baker[1,4], Olivier Morizot[1,5], Wolf von Klitzing[1,*]

1 *IESL-FORTH, Vassilika Vouton P.O. Box 1527, GR-71110 Heraklion Greece*

2 *Physics Department, University of Crete, GR711 03, Heraklion, Greece*

3 *Centre for Quantum Technologies, National University of Singapore, 3 Science Drive 2, 117542 Singapore*

4 *The University of Queensland, Brisbane St Lucia, QLD 4072, Australia*

5 *Université de Provence, Phys. des Interact. Ioniques et Moléculaires (UMR 6633), F -13397 Marseille Cedex 20, France*

Received 11 May 2012; accepted 7 July 2012

Abstract: Cold atom experiments often use images of the atom clouds as their exclusive source of experimental information. The most commonly used technique is absorption imaging, which provides accurate information about the shapes of the atom clouds, but requires care when seeking the absolute atom number for small atom samples. In this paper, we present an independent, absolute calibration of the atom numbers. We directly compare the atom number detected using dark-ground imaging to the one observed by fluorescence imaging of the same atoms in a magneto-optical trap. We normalise the signal using single-atom resolved fluorescence imaging. In order to be able to image the absorption of the very low atom numbers involved, we use diffractive dark-ground imaging as a novel, ultra-sensitive method of *in situ* imaging for *untrapped* atom clouds down to only 100 atoms. We demonstrate that the Doppler shift due to the acceleration of the atoms by the probe beam has to be taken into account when measuring the atom-number.

PACS (2008): 07.77.Gx,42.30.-d,42.30.Va, 39.90.+d,03.75.Be

Keywords: ultra-cold atoms • magneto optic trap • dark-ground imaging • absorption imaging

Cold atom experiments extract most of their experimental information from images of freely expanding atom clouds.

*E-mail: darkimaging@bec.gr (Corresponding Author)

In recent years the drive towards measurements of correlations, squeezing, and entanglement in one, two, or three dimensions has created a great need for better imaging techniques for very small atom samples [1–3]. Fluorescence detection has been demonstrated down to the sin-

gle atom level for trapped atoms [4] and more recently for atoms falling through a light sheet [5]. In the context of ultra-cold atoms and Bose-Einstein condensation (BEC), where the spatial distribution of atoms reveals most of the important physics, absorption imaging is the most commonly used technique. Recently, diffractive dark-ground imaging has been demonstrated as a novel ultra-sensitive technique to image very small ultra-cold atom sample [6].

Often, it is of great importance to detect the shape of an atom cloud also as well as its absolute atom number. A magneto-optic trap (MOT) can measure down to single atoms [7]. Unfortunately, it provides spatial information only about the average distribution of trapped atoms, and thus about the confining potential. Dark-ground imaging allows one to measure the shape of very small clouds, but fails to reach the single atom level. Ref. [6] provides a detailed analysis of the atom numbers detected using dark-ground and absorption imaging. In an experimental comparison between the two methods they found good agreement. Both the absorption and dark-ground imaging techniques, however, rely on exactly the same physics with respect to the scattering of the light by the atoms.

In this letter, we compare the atom number detected by fluorescence imaging in a magneto-optic trap (MOT) to the ones detected by absorption imaging. We normalise the fluorescence contribution per atom by observing the photon statistics of just a few atoms trapped in the MOT. In order not to affect the normalisation, we choose to keep the MOT parameters constant even for larger atom numbers. The atom density in this high-gradient MOT has to be kept well below any saturation limit, e.g. due to molecular association, resulting in samples which are far too small for standard absorption imaging techniques. We therefore employ dark-ground imaging—a novel ultra sensitive absorption imaging technique [6]. For each data-point, we determine the number of atoms from an image of the fluorescence of the atoms in the MOT, release the atoms, and take the dark-ground imaging sequence of the very same atom sample. We examine atom samples from two thousand down to a few hundred atoms.

The experimental setup (Fig. 1) consists of a fused-silica UHV cell, the MOT and imaging optics, and the field generating coils. The MOT traps from one to a few thousand ^{87}Rb atoms. The three retro-reflected MOT beams have an $1/e^2$ diameter of 3 mm and a saturation parameter of $s = 4$ per beam. The magnetic field gradient is 75 G/cm resulting in an average cloud size of about 15 µm. We use rubidium dispensers to control the pressure of ^{87}Rb in the vacuum cell, which enables us to reduce the atom number in the MOT down to single ^{87}Rb atoms with a trap-lifetime

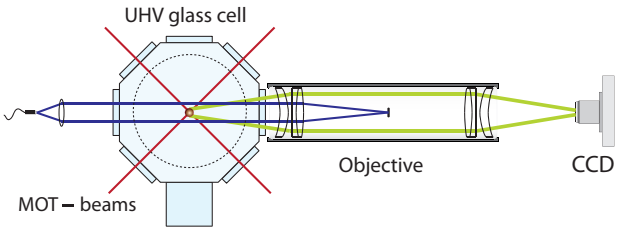

Figure 1. Schematic of the experimental setup. Three sets of retro-reflected beams (red) form a magneto-optic trap (MOT) inside a UHV glass cell. The field generating coils lie above and below the plane of the image. The fluorescence emitted from the MOT is collected by the relay objective and magnified onto the CCD camera. For dark-ground imaging the atoms are probed with a short pulse of a probe light (dark blue). The first lens collimates the diffracted light (green) but focuses the probe light. In the Fourier plane of the image, an opaque disk blocks the probe beam, but leaves the diffracted light virtually untouched. A second lens then forms a bright image of the atom cloud on a dark background, which is subsequently magnified onto the CCD camera by a microscope objective.

of up to 13 s. This allows us to directly detect the fluorescence level of a single atom as an *absolute normalisation* of the atom number in the MOT. We determine the single atom fluorescence from the histogram of the photon counts of a low atom MOT. For this we take a number of fluorescence images of a MOT containing just a few atoms ($\tau_{exp} = 0.5$ s). We then fit a 2D-Gaussian to each image and use it to calculate the integrated photon counts. We then fit Gaussians to the resulting histograms of the photon counts (see for example Fig. 2). The fit to the first and second non-zero peak then serves as a normalisation for the fluorescence images of larger clouds. We estimate the uncertainty due to long-term drifts at about 15%.

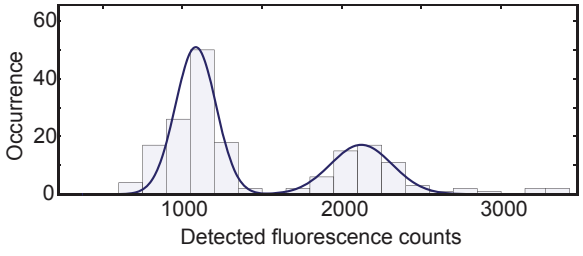

Figure 2. Histogram of the integrated photon counts on the CCD camera of 300 successive fluorescence images in a MOT. The first non-zero peak corresponds to a single atom and the second to two atoms.

Dark-ground imaging uses an optical Fourier transform filter to selectively remove the light of the probe beam from the image. This reduces the noise from the large background of the probe light, thus enabling us to image

atom clouds with only 100 atoms at optical depths[1] down to OD = 0.01 using an exposure time of 100 µs. The principles of diffractive dark-ground imaging are described in [6]. Fig. 1 shows the experimental setup used here. The collimated probe beam (blue lines) is partially absorbed by a small atom cloud thus forming a dark region on a bright background. The image of the cloud then diffracts (green lines) until it reaches the first lens, which collimates the diffracted light but focuses the remaining light of the probe beam. A small dark spot placed at the focus of the first lens then blocks the probe beam but leaves virtually untouched the collimated diffraction of the atom cloud. A second lens then images the light onto a camera, where the atom cloud appears as a bright object on a dark background. By removing the probe light from the final image, diffractive dark-ground imaging filters out much of the noise that is contained within this background thus allowing the detection of far lower atom numbers. A typical imaging sequence contains three images: First we take the dark-ground image (I_{dark}) with the atoms and the probe light present, then the reference image without the atoms (I_{ref}), and finally the background image (I_{bgr}). We then calculate the transmission $T = (I_{\mathrm{dark}} - I_{\mathrm{bgr}})/(I_{\mathrm{ref}} - I_{\mathrm{bgr}})$. The atom column density n is then

$$n = \frac{2}{\sigma}\left(\sqrt{T + \Omega^2} - \Omega\right), \qquad (1)$$

where Ω is the fluorescence detection efficiency and $\sigma = \sigma_0/(1 + s + 4\delta^2/\Gamma^2)$ the atomic absorption cross section including corrections for the laser detuning and saturation, with $\sigma_0 = 2.503\,\mathrm{mW/cm^2}$ [8]. Figure 3 shows examples of dark-ground images of 115 to 1800 atoms.

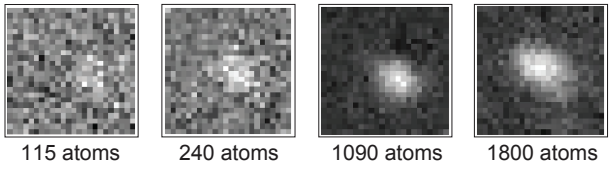

Figure 3. Dark-ground images of clouds with various atom numbers taken with an illumination time of 100 µs. The reference images have been subtracted from the raw images. The size of the frames is 80 × 80 µm in the object plane. The atom numbers are determined from the corresponding fluorescence images.

The objective in Fig. 1 is used for both fluorescence and diffractive dark-ground images and consists of two identical sets of lenses at a distance of two focal lengths (f).

[1] *We define the optical depth as the natural logarithm of the transmittance through the atom cloud.*

The dark spot is located in the Fourier plane of the image, exactly in the middle between the two sets of lenses ($4f$-configuration) and consists of an AR-coated window with a circular chromium spot of 200 µm diameter at its centre. The resulting image is then magnified ×4 by a microscope objective and imaged onto the CCD of the camera. The total imaging system has a numerical aperture of $NA = 0.1$ and a diffraction limited resolution of 9 µm. The CCD camera (Andor iKon-M 934BR-DD) has a quantum efficiency of 95% at 780 nm and a pixel size of 13 µm resulting in a pixel size of 3.25 µm in the object plane. The transmission of the optics including the window of the cell is 84% resulting in a total fluorescence detection efficiency of $\Omega = 0.002$. For both trapping and imaging, we use the cycling transition $F = 2 \rightarrow F' = 3$ of the D-2 line and a weak repumper (5% of total) at $F = 1 \rightarrow F' = 2$. For the dark-ground imaging we use σ-polarised light.

In choosing the size of the dark spot, care has been taken to block the probe beam as much as possible without significantly attenuating the diffracted light. The light diffracted by a cloud of Gaussian shape expands like a Gaussian beam according to $w(z) = w_0\sqrt{1 + (z/z_{\mathrm{R}})^2}$, where $z_{\mathrm{R}} = \pi w_0^2/\lambda$ is the Rayleigh range. The first set of lenses collimates this beam which then travels past the dark spot. For a typical atom-cloud of a radius of $w_0 = 15$ µm and a dark spot of 100 µm radius we calculate a loss of the image intensity of only 2%. The radius of our imaging beam of $w_0 \geq 0.5$ mm results in a focal spot of $w_0 \leq 47$ µm, which matches our measured extinction ratio of 800. Larger dark spots result in higher extinction ratios, at the cost of increasing the losses in the image intensities of larger clouds. Larger probe beams, on the other hand, result in an increased background due to scattering. In order to prevent a change in the size of the atom cloud during the dark-ground imaging, we choose the exposure time ($\tau = 100\mu s$) short enough, so that the transverse diffusion ($\Delta\rho = v_{\mathrm{rec}}\sqrt{R_{\mathrm{sc}}\tau^3/3}$) is small compared to the radius of the atom cloud (w_0). With v_{rec} as the recoil velocity and R_{sc} as the scattering rate we find for our typical parameters a diffusion of $\Delta\rho \simeq 7$ µm, which is smaller than our cloud radii of $w_0 \simeq 15$ µm.

A comparison between the atom number measured by fluorescence to the one determined by dark-ground imaging can be seen in Fig. 5. The imaging procedure commences by taking a fluorescence image of the trapped atoms with an exposure time of 0.5 s. We then switch off the trap, wait 1 ms, and acquire a sequence of three images: the dark-ground, reference, and background image. We use an exposure time of $\tau = 100$ µs at a saturation parameter of $s = 2.5$ and a detuning of $\delta = +0.7\,\Gamma$. The delay between the images in the dark-ground sequence is 400 µs. The atom number found from each dark-ground image is

Event	Duration
Fluorescence Image in MOT	500ms
Switch off MOT	0.1ms
Free Expansion	1ms
Dark Ground Image	0.1ms
Wait	0.4ms
Reference Image	0.1ms
Wait	0.4ms
Background Image	0.1ms

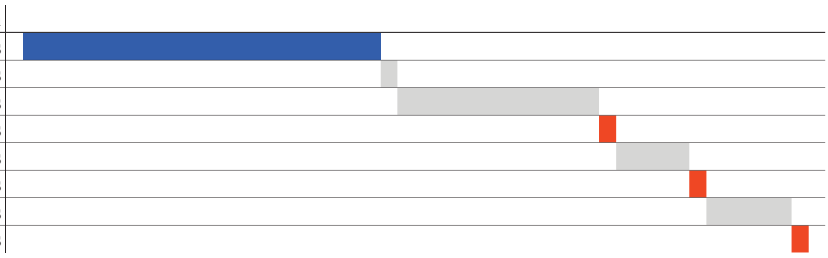

Figure 4. The imaging Sequence: Fluorescence Imaging in the MOT (blue) and Dark-Ground Imaging (red) of the untapped atoms.

compared directly to the one from fluorescence image of the same atom cloud. Fitting a straight line to the data, we find that the atom number detected by dark-ground imaging is about 24% larger than the one of fluorescence imaging.

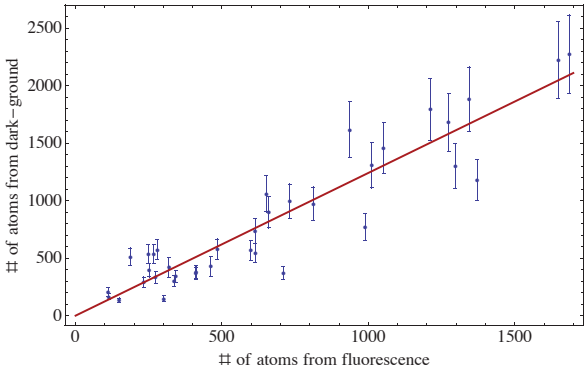

Figure 5. Atom number measured by the dark-ground imaging as a function of the atom number determined by fluorescence imaging. The solid line is a straight line fit to the data resulting in a slope of 1.24 ± 0.08 atoms per atom and an offset of 1 ± 66 atoms. At a detuning of $+0.7\,\Gamma$, a saturation of $s = 2.5$, and an exposure time of $100\,\mu s$ the correction factor due to the Doppler shift is 0.77 resulting in a final slope of 0.96 ± 0.06. The quoted errors are standard errors of the fit. The uncertainty in the fluorescence detection is about 15%.

We attribute this 24% increase in the atom numbers detected by dark-ground imaging to the fact that the light from the probe beam accelerates the atoms during the imaging pulse; thus Doppler-shifting the probe light closer to resonance. We calculate this increase in scattering due to the Doppler shift by determining first the change in velocity due to the imaging beam and then averaging the reduced scattering over the imaging time. The scattering rate including the Doppler-shift is [9]:

$$\Gamma_{\text{scatter}} = \frac{\Gamma}{2}\frac{s}{1+s+4(\delta - kv)^2/\Gamma^2} \qquad (2)$$

where v is the velocity of the atoms, $k = 2\pi/\lambda$ the wavevector of the imaging beam, δ the detuning from the transition in units of radians/s, and Γ the natural full line width of the transition. We determine the velocity of the atoms as a function of exposure time solving the differential equation for the acceleration $a = \hbar k \Gamma_{\text{scatter}}/m$. We then insert the time dependent velocity into Eq. 2 and integrate numerically over the exposure time. For our experimental parameters this results in a increase of the signal by 30%.

Applying the Doppler-correction to the experimental data of Fig. 5 we find good agreement between the atom number determined using dark-ground imaging and the one from fluorescence imaging: $dark/fluo = 0.96 \pm 0.16$. The error is dominated by the uncertainty in the atom number detected by fluorescence imaging (15%).

It is interesting to note that the same correction applies to any form of absorption imaging. For example, for the standard resonant absorption imaging with a saturation parameter of only $s = 0.1$ and an exposure time of $\tau = 100\,\mu s$ we calculate a reduction of the absorption signal by 5% due to the acceleration of the atoms by the probe beam.

In summary, we have compared for the first time dark-ground and fluorescence imaging in a MOT for cold-atom clouds of 1000 atoms down to only 100 atoms. We find good agreement between the two methods only after taking into account the Doppler shift caused by the acceleration of the atoms by the imaging beam.

This work has been supported by a Marie Curie Excellence Grant of the European Community (MEXT-CT-2005-024854). We would like to thank Giorgos Konstantinidis for supplying early versions of the dark-spot.

References

[1] J. Estève, C. Gross, A. Weller, S. Giovanazzi, M. Oberthaler, Nature 455, 1216 (2008)

[2] F. Gerbier, S. Fölling, A. Widera, O. Mandel, I. Bloch, Phys. Rev. Lett. 96, 90401 (2006)
[3] S. Folling, F. Gerbier, A. Widera, O. Mandel, T. Gericke, I. Bloch, Nature 434, 481 (2005)
[4] Z. Hu and H. Kimble, Opt. Lett. 19, 1888 (1994)
[5] R. Bücker et al., New J. Phys. 11, 103039 (2009)
[6] M. Pappa et al., New J. Phys. 13, 115012 (2011)
[7] D. Haubrich, H. Schadwinkel, F. Strauch, B. Ueberholz, R. Wynands, D. Meschede, Europhys. Lett. 34, 663 (1996)
[8] D. Steck, Rubidium 87 D line data (University of Oregon, 2010)
[9] C. Foot, Atomic physics (Oxford University Press, 2005)